

A New Way of Controlling Parallel-Connected Inverters by Using Synchronous-Reference-Frame Virtual Impedance Loop—Part I: Control Principle

Yajuan Guan, *Student Member, IEEE*, Josep M. Guerrero, *Fellow, IEEE*, Xin Zhao, Juan C. Vasquez, *Senior Member, IEEE*, and Xiaoqiang Guo, *Senior Member, IEEE*

Abstract—A novel simple and effective autonomous current-sharing controller for parallel three-phase inverters is proposed in this paper. The proposed controller provides faster response and better accuracy in contrast to the conventional droop control, since this novel approach does not require any active or reactive power calculations. Instead, a synchronous-reference-frame (SRF) virtual impedance loop and an SRF-based phase-locked loop are used. Stationary analysis is provided in order to identify the inherent mechanism of the direct and quadrature output currents in relation to the voltage amplitude and frequency with different line impedances by means of the system transfer functions. Comparison experiments from two parallel inverters are presented to compare the control performance of the conventional droop control and the proposed control with different line impedances. In addition, experimental results from a setup with three parallel 2.2-kW inverters verify the effectiveness of the proposed control strategy in different scenarios.

Index Terms—Droop control, parallel inverters, phase-locked loop (PLL), synchronous reference frame, virtual impedance.

I. INTRODUCTION

DROOP control method has been widely used in the last decade as the decentralized control of parallel converters in several applications, such as parallel redundant uninterruptible power supplies (UPS) to avoid critical communication among units, distributed power systems, microgrids (MGs), etc [1]–[12]. This well-known control technique aims to proportionally share active and reactive powers with adjusting frequency and output voltage amplitudes of each inverter locally in order to emulate the behavior of a synchronous generator [3]. Although this technique only requires local information, it presents a number of stability issues that have been solved along the literature [4]–[7].

One of the main problems is that the droop coefficients which regulate frequency and amplitudes are basically proportional terms so that in order to increase their range of values for

improving system dynamics, derivative terms were added [13]–[16]. Unlike the conventional droop controllers which yield one dimension of freedom (DOF) tunable control, the improved droop controllers yield 2-DOF tunable control. Subsequently, the dynamic performance of the system can be adjusted to damp the oscillatory behavior of the power-sharing controllers without affecting the static droop gains.

Another issue with regards to conventional droop is that the frequency and voltage are, respectively, related to active and reactive power when the output impedance of the generator is mainly inductive, e.g., induction generators. Hence, by using the droop method, the power-sharing performance is affected by the output impedance of the distributed generation (DG) units and the line impedances. However, the output impedance can be fixed by means of a fast control loop named virtual impedance in an inverter [17], [18]. In this sense, the output impedance can be treated as another control loop which enforces the inverter to behave in accordance to the inductance-to-resistance ratio (X/R) line impedance, e.g., mainly resistive in case of low-voltage networks [19].

In case of resistive lines and/or virtual impedances, the active power is controlled by the inverter voltage amplitude, while the reactive power flow is dominated by the angle so that it can be controlled by the frequency of the system [20]–[24]. In this sense, the active power–voltage ($P-V$) droop control needs to be used instead of the conventional active power–frequency ($P-f$) droop control, which is contrary to the conventional electrical transmission systems or induction-generation dominated systems.

Several control methodologies with different implementations for a conventional droop controller have also been proposed [25]–[28]. A $Q-V$ dot droop control method is mostly used to improve the reactive power sharing [29].

Based on the aforementioned issues, a control architecture based on a virtual resistance, $P-V$ and $Q-f$ droops are used for dealing with the autonomous operation of parallel-connected inverters [20], [30]. However, this approach has the inherent drawback that it needs to calculate instantaneous active and reactive powers, and then, average them through low-pass filters (LPFs) whose bandwidth deteriorate the system transient response [15]. Even in three-phase systems that the active and reactive power can be calculated by using the instantaneous power theory, a postfilter processing is necessary in order to completely remove the distorted power components [31]. Furthermore, in a practical situation, the load-sharing performance

Manuscript received March 26, 2015; revised July 2, 2015; accepted August 7, 2015. Date of publication August 25, 2015; date of current version January 7, 2016. Recommended for publication by Associate Editor F. Gao.

Y. Guan, J. M. Guerrero, X. Zhao, and J. C. Vasquez are with the Department of Energy Technology, Aalborg University, Aalborg 9220, Denmark (e-mail: ygu@et.aau.dk; joz@et.aau.dk; xzh@et.aau.dk; juq@et.aau.dk).

X. Guo is with the Key Laboratory of Power Electronics for Energy Conservation and Motor Drive, Department of Electrical Engineering, Yanshan University, Qinhuangdao 066004, China (e-mail: gxq@ysu.edu.cn).

Color versions of one or more of the figures in this paper are available online at <http://ieeexplore.ieee.org>.

Digital Object Identifier 10.1109/TPEL.2015.2472279

of the conventional droop control is degraded when short lines with small impedance are used, especially in low-voltage networks. In this case, a small deviation in voltage frequency and amplitude will result in large power oscillation and even instabilities [32]. The drawbacks of droop control can be summarized as follows:

- 1) *slow dynamic response*: since it requires LPFs with reduced bandwidth to calculate the average values of the active and reactive powers both in islanded and grid-connected modes;
- 2) active/reactive power coupling;
- 3) slow responses when active/reactive power-sharing ratios are suddenly changed;
- 4) performance is strongly affected by the line impedance;
- 5) complex design;
- 6) the power sharing could be degraded if the sum of the output impedance and the line impedance is unbalanced.

Another possible solution is the combination of current sharing control and power droop control techniques. A voltage-power droop/frequency-reactive power boost control scheme which allows multiple voltage-source converters to operate in parallel in MGs and to share a common load power in proportion to a predetermined ration is presented in [33] and [34]. In [33], an additional virtual resistance loop is necessary since the inverter output impedance cannot be equal to zero due to the PI controller in voltage control loop. A decentralized control for redundant parallel connection of multiple UPS using only current sensors is proposed [35], [36]. The active and reactive components of output current are used instead of active and reactive power to mimic the droop control, while the LPFs are still necessary. A novel piecewise linear V - I droop controller has been proposed to exploit the flexibility and fast dynamics of the inverter-based distributed energy resources [37]. However, a global positioning system signal as the communication is used to synchronize each DG unit and allow for constant frequency operation. A voltage and frequency droop control based on mixed voltage and current source concept and finite output impedance emulation for single-phase inverter-based low voltage grid has been proposed [22], [38]. This method can provide not only wireless parallel operation control, but also has the capability of mitigation of voltage harmonics and short-circuit behavior as it takes the R to X line impedance ratio into account. However, this control approach is complex, since a Kalman filter estimator and a linear quadratic regulator are required.

To cope with all the aforementioned, a simpler and faster controller is proposed in this paper, which consists of a synchronous-reference-frame (SRF) virtual impedance loop, an SRF phase-locked loop (PLL), and a proportional-resonant (PR) controller in voltage control loop. The proposed control strategy provides both instantaneous current sharing and fast dynamic response for paralleled-voltage-controlled inverters (VCIs). The virtual resistance loop which contains a d -axis virtual resistance loop and a q -axis virtual resistance loop is used to achieve direct and quadrature load currents sharing separately among three-phase inverters. The concept is derived from the current-sharing control schemes already used in dc-paralleled converters [39]–[42]. In contrast with the conventional droop control, there is no need to calculate active/reactive powers. An additional PLL

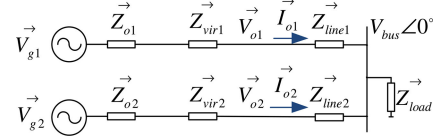


Fig. 1. Equivalent circuit of a parallel-inverter system with virtual resistances.

is needed to adjust the phase of the voltage reference and to ensure the synchronization among the paralleled VCIs. The paper is organized as follows. Section II reviews the conventional droop control principle. Section III analyzes the current flow when virtual resistive impedance in the stationary reference frame is used. Section IV introduces the proposed control structure and the control principle. Section V presents the inherent droop characteristic and coupling analysis of the proposed control with different line impedances. Experimental results are shown in Section VI in order to evaluate the feasibility of the proposed approach and to compare the control performance with the conventional droop control. Section VII concludes this paper. Finally, the appendix provides the derivative process of the mathematic equations. This paper is the first part of a two-part paper focusing on the control principle and steady-state performance analysis. The second part of this paper deals with the small-signal state-space models and stability analysis of the proposed parallel-VCI-based system.

II. REVIEW OF THE DROOP CONTROL PRINCIPLE

Fig. 1 shows the equivalent circuit of a two-paralleled inverter system including generated voltages (\vec{V}_{g1} and \vec{V}_{g2}), output impedances (\vec{Z}_{o1} and \vec{Z}_{o2}), virtual impedances (\vec{Z}_{vir1} and \vec{Z}_{vir2}), output voltage (\vec{V}_{o1} and \vec{V}_{o2}), and line impedances (\vec{Z}_{line1} and \vec{Z}_{line2}) of each inverter. It can be considered as a subset of distributed power network operating in an autonomous islanded mode.

The phase differences between the output voltage (φ_{gn}) and the point of common coupling voltage (φ_{bus}), as well as the amplitude of equivalent impedance ($Z_n \angle \varphi_n$), which consists of inverter output impedance ($Z_{on} \angle \varphi_{on}$), line impedance ($Z_{line} \angle \varphi_{line}$), and virtual impedance ($Z_{vir} \angle \varphi_{vir}$), are considered in this study. The active and reactive power output can be derived as

$$P_n = \frac{V_{gn}^2 \cos \varphi_n - V_{gn} V_{bus} \cos(\varphi_{gn} - \varphi_{bus} + \varphi_n)}{Z_n} \quad (1)$$

$$Q_n = \frac{V_{gn}^2 \sin \varphi_n - V_{gn} V_{bus} \sin(\varphi_{gn} - \varphi_{bus} + \varphi_n)}{Z_n} \quad (2)$$

In traditional power systems, the equivalent impedances between the paralleled inverters present high X/R ratio. The active power (P_n) can be adjusted with the voltage angle (φ_{gn}), and reactive power (Q_n) can be regulated with voltage amplitude (V_{gn}) separately. Based on this power flow analysis, the droop control law can be expressed as

$$\omega_n = \omega_n^* + k_{p\omega} (P_n^* - P_n) \quad (3)$$

$$V_n = V_n^* + k_{qV} (Q_n^* - Q_n) \quad (4)$$

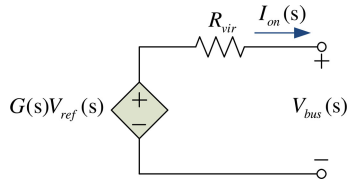


Fig. 2. Equivalent Thévenin circuit of a closed-loop inverter.

where ω_n^* and V_n^* are the normal angular frequency and output voltage amplitude, respectively, and $k_{p\omega}$ and k_{qV} are the droop coefficients.

However, the load-sharing performance of the conventional droop control is degraded in a practical situation when using short lines with small impedances, especially in low-voltage networks. Output power (P_n and Q_n), output voltage amplitude and frequency are coupled, because $[\sin(\varphi_{on} - \varphi_{bus})]/Z_n \approx (\varphi_{on} - \varphi_{bus})/Z_n$ cannot be neglected when $\varphi_n - \varphi_{bus} \neq 0$ or Z_n is too small, that may result in imprecise power control. Furthermore, the stability problems would arise for conventional droop controlled systems with small equivalent line impedance Z_n , since small frequency or voltage amplitude deviations can result in large power oscillations.

III. CURRENT FLOW ANALYSIS

Each inverter in Fig. 1 can be modeled by a two-terminal Thévenin equivalent circuit in Laplace as follows:

$$V_{bus}(s) = G_n(s)V_{refn}(s) - [Z_{on}(s) + Z_{linen}(s) + Z_{virn}(s)] \times I_{on}(s) \quad (5)$$

where $V_{refn}(s)$ is the output voltage reference, and $G_n(s)$ is the voltage gain. The inner current and voltage loops are responsible for minimizing $Z_{on}(s)$, i.e., by using a PR controller tuned at the line frequency. In this sense, $Z_{on}(s)$ is approximately equal to zero, whereas $G_n(s)$ is equal to 1 at the resonant frequency of a PR controller.

Considering that $Z_{linen}(s)$ is practically very small in low-scale systems, such as low-voltage MGs, $Z_{virn}(s)$ becomes the predominant component. Thus, (5) can be simplified as

$$V_{bus}(s) = G_n(s)V_{refn}(s) - Z_{virn}(s)I_{on}(s). \quad (6)$$

When only virtual resistance is adopted, an equivalent Thévenin circuit can present the closed-loop inverter, as illustrated in Fig. 2. The voltage difference between the generated voltage and common bus voltage at the line frequency can be expressed in dq reference frame as follows:

$$\vec{V}_{refn} - \vec{V}_{bus} = I_{odn}R_{vir dn} + jI_{oqn}R_{vir qn} \quad (7)$$

where I_{odn} and I_{oqn} are the d - and q -axis components of output current, respectively.

In this case, because the voltage reference phasor (\vec{V}_{ref}) and common bus voltage phasor (\vec{V}_{bus}) are identical for each DG unit, the different values of $R_{vir d}$ and $R_{vir q}$ will result in different voltage drops that will cause different current output vectors

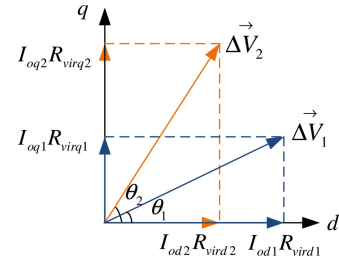


Fig. 3. Vector diagram of the concept.

(\vec{I}_o), as shown in Fig. 3. The relationship of I_{od} , I_{oq} , $R_{vir d}$, and $R_{vir q}$ can be generalized and expressed for number N of converters as follows:

$$I_{od1}R_{vir d1} = I_{od2}R_{vir d2} = \dots = I_{odN}R_{vir dN} \quad (8a)$$

$$I_{oq1}R_{vir q1} = I_{oq2}R_{vir q2} = \dots = I_{oqN}R_{vir qN}. \quad (8b)$$

The d - and q -axis output currents I_{od} and I_{oq} of the paralleled inverters are inversely proportional to the corresponding virtual resistances. Therefore, the direct and quadrature output of each inverter can be regulated independently by adjusting the virtual impedances based on different power rates, commands from energy management system (EMS) or other superior control loops.

Furthermore, the active and reactive power output sharing strategy among the paralleled inverters can be obtained from (8) by multiplying the voltage reference. Hence, considering that the voltage references (V_{ref}) of each inverter are equal, the active and reactive power output will also be properly shared based on the virtual resistances as

$$P_{o1}R_{vir d1} = P_{o2}R_{vir d2} = \dots = P_{oN}R_{vir dN} \quad (9a)$$

$$Q_{o1}R_{vir q1} = Q_{o2}R_{vir q2} = \dots = Q_{oN}R_{vir qN} \quad (9b)$$

where P_{on} and Q_{on} are the active and reactive power output of inverter $\#n$.

IV. PROPOSED AUTONOMOUS CURRENT-SHARING CONTROLLER

Follow the above analysis, a simpler and faster controller is proposed in this paper. The novel control strategy is shown in Fig. 4(b). Compared with the improved droop controller in Fig. 4(a), the droop controller could be replaced by a novel controller which comprises of an SRF-PLL and a virtual resistance loop in SRF.

A. Configuration of the Proposed Controller

The power stage consists of a three-leg three-phase inverter connected to a dc link, loaded by an $L_f - C_f$ filter, and connected to the ac bus through a power line (Z_{line}). Indeed, the proposed control strategy can also be extended to single-phase systems. The main difference between the single-phase systems and three-phase systems is that the orthogonal voltage system in

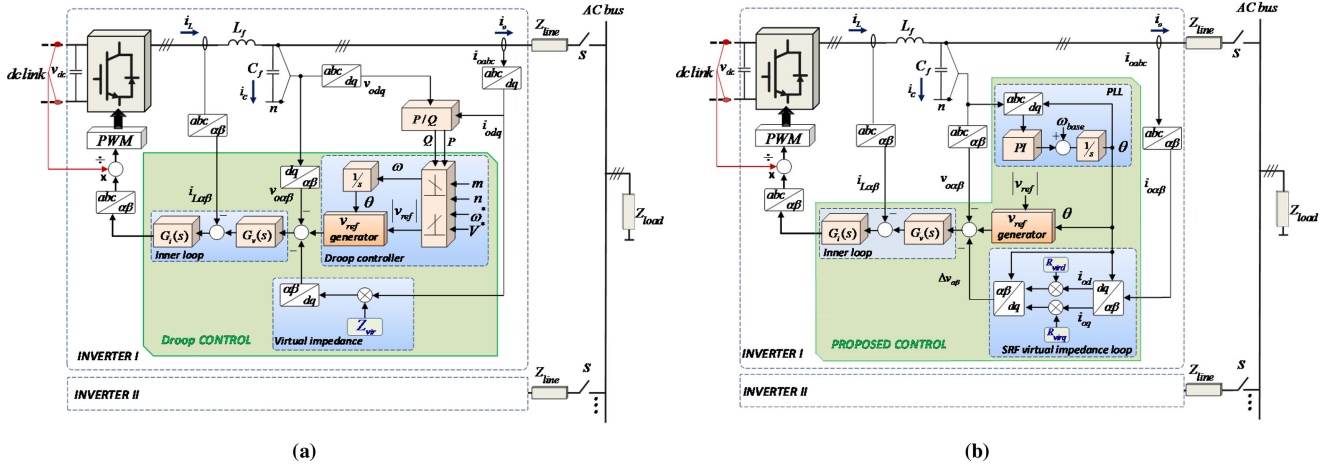


Fig. 4. Control structure comparison between (a) the conventional droop control and (b) the proposed control method.

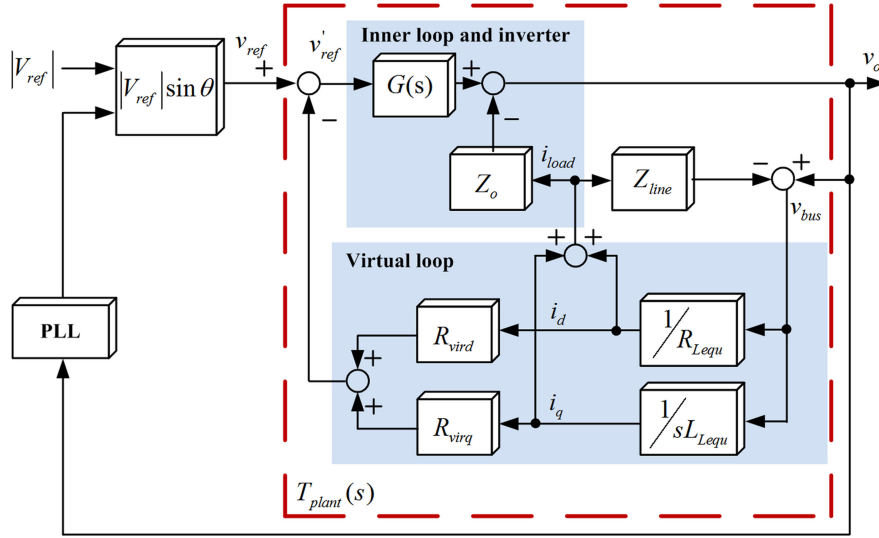


Fig. 5. Simplified control block diagram.

single-phase systems needs to be generated by an extra control loop [43], [44].

The controller including an SRF-PLL, a virtual resistance loop ($R_{vir d}$ and $R_{vir q}$), a dc-link voltage feed-forward loop, and the conventional PR inner voltage and current controllers (G_v and G_i) generates a PWM signal to drive the IGBT inverter gates. Inductive currents and capacitor voltages are transformed to the stationary reference frame ($i_{L\alpha\beta}$ and $v_{c\alpha\beta}$). Output currents are transformed to the SRF (i_{odq}). The direct and quadrature output currents are independently controlled by the virtual impedance loop in dq axis. The inner voltage and current loops are implemented in $\alpha\beta$ reference frame since the PR controller can deal with both positive- and negative-sequence voltage when the negative sequence voltage and current appear.

Fig. 5 shows the simplified proposed control block diagram, which includes the three-leg three-phase inverter $L_f - C_f$ filter, line impedance, virtual impedance loop, the PLL, and the inner voltage and current control loops.

The closed-loop transfer function $T_{plant}(s)$ can be described as follows:

$$T_{plant}(s) = \frac{V_o(s)}{V_{ref}(s)} = \frac{G(s) [1 + G_{Lequ}(s)Z_{line}(s)]}{1 + G_{Lequ}(s)Z_{line}(s) + G_{vir}(s)G(s) + G_{Lequ}(s)Z_o(s)} \quad (10)$$

being

$$G(s) = \frac{G_v(s)G_i(s)K_{PWM}}{L_f C_f s^2 + (rC_f + G_i(s)K_{PWM}C_f)s + 1 + G_v(s)G_i(s)K_{PWM}}$$

$$Z_o(s) = \frac{sL_f + r}{L_f C_f s^2 + (rC_f + G_i(s)K_{PWM}C_f)s + 1 + G_v(s)G_i(s)K_{PWM}}$$

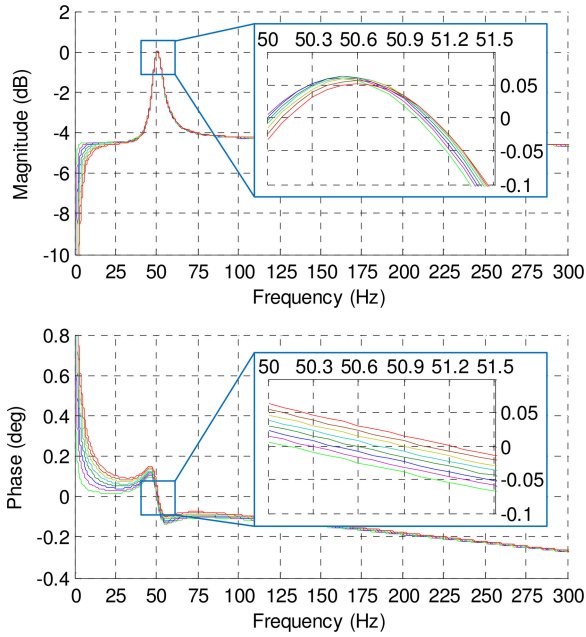


Fig. 6. Bode diagram of the system transfer function.

$$G_v(s) = K_{pv} + \frac{K_{iv}s}{s^2 + \omega_c^2}, G_i(s) = K_{pi}, G_{Lequ}(s) = \frac{1}{R_{Lequ}} + \frac{1}{sL_{Lequ}}$$

$$Z_{line}(s) = R_{line} + sL_{line}, G_{vir}(s) = \frac{R_{vir d}}{R_{Lequ}} + \frac{R_{vir q}}{sL_{Lequ}}$$

where $G(s)$ presents the tracking performance of the output voltage following the voltage reference, $Z_o(s)$ is the equivalent output impedance of the inverter, $Z_{line}(s)$ is the line impedance, R_{line} is the line resistor, L_{line} is the line inductance, $G_{Lequ}(s)$ is the equivalent load admittance, R_{Lequ} is the equivalent resistor, L_{Lequ} is the equivalent inductance, $V_o(s)$ is the output voltage, $V_{ref}(s)$ is the reference voltage, $i_o(s)$ is the output current, $G_v(s)$ is the PR voltage control loop, $G_i(s)$ is the proportional current control loop, K_{PWM} is the gain of three phase inverter, L_f , C_f , and r are the inductor, capacitor, and inductor ESR of the LC filter, respectively, K_{pv} and K_{iv} are the proportional and integral coefficients of the voltage control loop, ω_c is the resonant frequency of the PR voltage control loop, K_{pi} is the proportional coefficients of the current control loop, and $R_{vir d}$ and $R_{vir q}$ are the d -axis and q -axis virtual resistors.

The detailed derivative process is provided in the Appendix.

B. Control Principle

The proposed controller supplies a reference voltage to the inner loop. The voltage reference \vec{V}_{ref} is generated by combining the amplitude reference ($|V_{ref}|$) and the phase generated (θ) by the PLL.

Even though the PLL is trying to synchronize the inverter with common ac bus, in case of supplying reactive loads, the

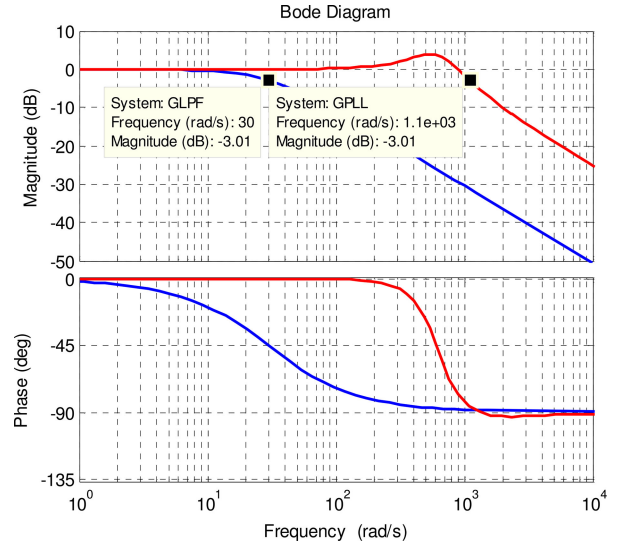


Fig. 7. Bode diagram of the PLL (red line) and the LPF (blue line).

quadrature current flowing through the virtual resistance will produce an unavoidable quadrature voltage drop, which will cause an increase in PLL frequency. In other words, the PLL will compel the inverter to be stabilized at a frequency point with zero phase delay (ZPD) obtained from the system transfer function. The frequency of ZPD is affected by the quadrature current as shown in Fig. 6. Thus, the mechanism inherently endows an $I_{oq} - \omega$ droop characteristic in each inverter.

Similarly, in case of supplying active loads, the direct current flowing through the virtual resistance will drop the direct voltage, causing a decrease in the output voltage amplitude. Hence, a droop characteristic is also imposed by the virtual resistance adapting the amplitude of output voltage, which endows to the system an $I_{od} - V$ droop characteristic.

Moreover, the settling time can be considerably improved because the proposed controller does not require any power calculation. The bandwidth of the PLL can be designed through the linearized model [45], [46] to be higher than the bandwidth of the LPF that is used for PQ calculation purposes in the conventional droop controller [47]. The cut-off frequency of the LPF in the power droop control loop is usually preassigned to 30 rad/s to obtain the average power, while avoiding undesirable interaction [45], [46]. The bandwidth of the PLL in the proposed control is 1100 rad/s when k_{pPLL} and k_{iPLL} are equal to 1.4 and 1000, respectively. The Bode diagram is shown in Fig. 7. However, the fastest transient response of PLL should be almost equal to the transient response speed of the inner voltage control loop to ensure the system stability.

V. INHERENT DROOP CHARACTERISTIC AND COUPLING ANALYSIS

Considering the inherent mechanism of I_{od} with voltage amplitude and I_{oq} with frequency, two virtual resistances $R_{vir d}$ and $R_{vir q}$ are employed to share the quadrature and direct load currents among the inverters individually.

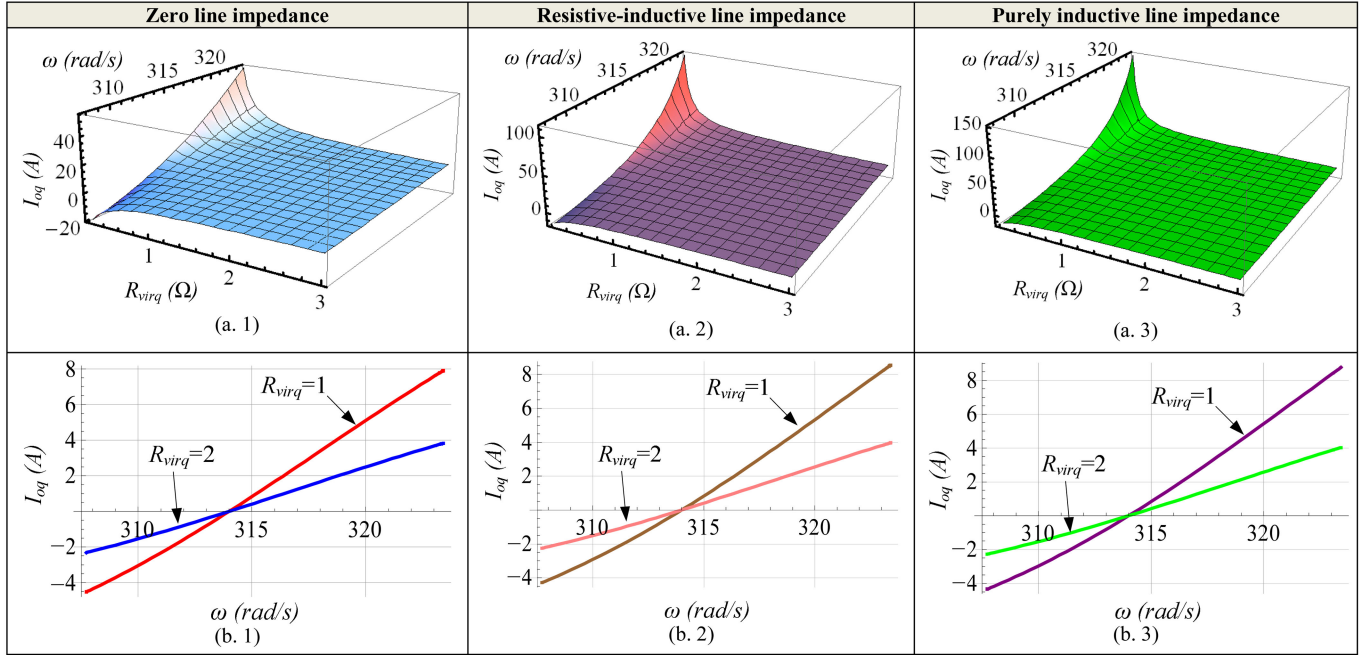


Fig. 8. Relationship of R_{virq} , I_{oq} , and ω with different line impedances. (a) Relationship of R_{virq} , I_{oq} , and ω with different line impedances. (b) Relationship of I_{oq} and ω when $R_{virq} = 1\Omega/2\Omega$ with different line impedances.

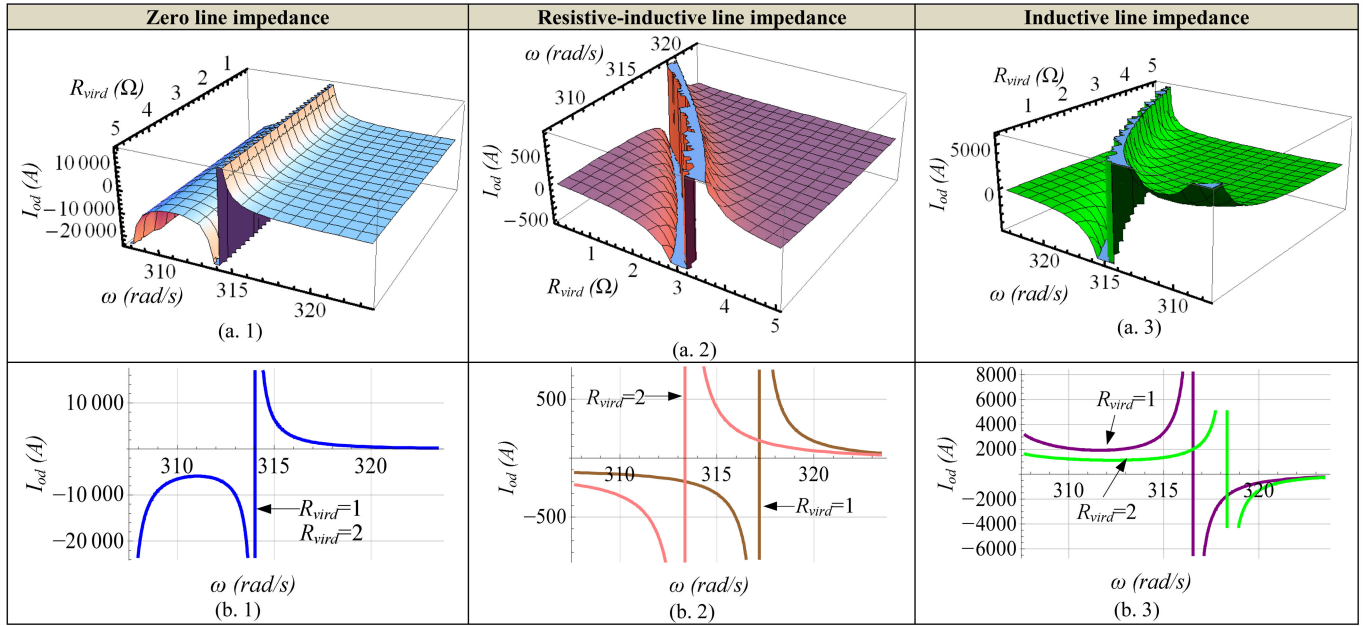


Fig. 9. Relationship of R_{vird} , I_{od} , and ω with different line impedances. (a) Relationship of R_{vird} , I_{od} , and ω with different line impedances. (b) Relationship of I_{od} and ω when $R_{vird} = 1\Omega/2\Omega$ with different line impedances, respectively.

A. I_{oq} Sharing

When the inverters and loads all connect to the common ac bus, the proposed controller will make the system stable at a frequency-stable operation point which may has a small deviation from 50 Hz. The small deviation is determined by the function of PLL, R_{virq} , and I_{oq} . The frequency-stable operation should be the cross zero point of the phase-frequency characteristics of the closed-loop transfer function of the system, as depicted in the dashed part in Fig. 5.

Therefore, the parallel inverters will operate on the same system frequency, but with different phase angles that depend on the output quadrature current and q -axis virtual resistance value.

Based on (10), as $s = j\omega$, the relationship of R_{vird} , R_{virq} , I_{od} , I_{oq} , and angular frequency (ω) can be calculated based on

$$\arctan [T_{plant}(j\omega)] = 0^\circ. \quad (11)$$

In order to analyze the relationship of R_{virq} , I_{oq} , and ω , R_{vird} and I_{od} are preset to fixed values. The relationship of

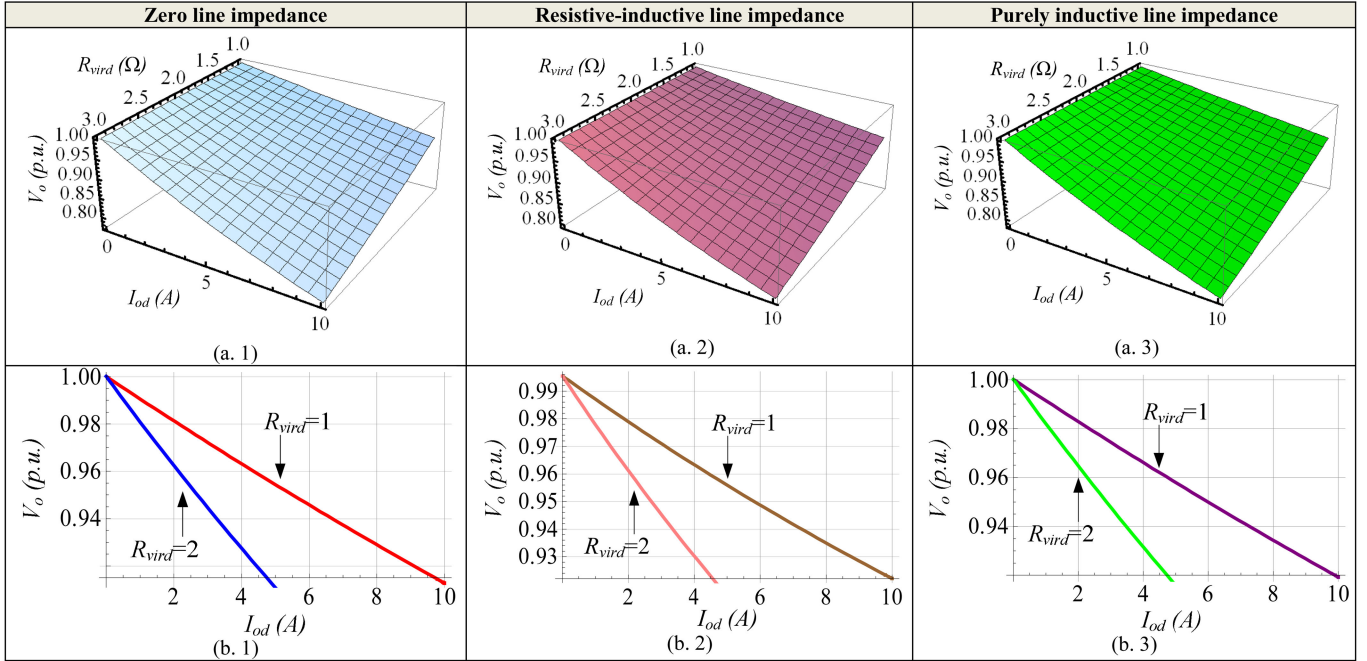


Fig. 10. Relationship of R_{vird} , I_{od} , and V_o with different line impedances. (a) Relationship of R_{vird} , I_{od} , and V_o with different line impedances. (b) Relationship of I_{od} and V_o when $R_{vird} = 1\Omega/2\Omega$ with different line impedances, respectively.

R_{virq} , I_{oq} , and ω with different line impedances is shown in Fig. 8. Fig. 8(a.1) and (b.1) shows the relationship with zero line impedance. Fig. 8(a.2) and (b.2) describes the relationship with resistive–inductive line impedance ($L_{line} = 1.7$ mH, $R_{line} = 1$ Ω). Fig. 8(a.3) and (b.3) presents the relationship with purely inductive line impedance ($L_{line} = 1.8$ mH). The inherent mechanism of the proposed $I_{oq} - \omega$ droop controller with different line impedances is depicted in Fig. 8(b.1)–(b.3). Fig. 8 indicates that the line impedances in this range barely have effect on the relationship of R_{virq} , I_{oq} , and ω , as well as $I_{oq} - \omega$ droop characteristics. This is because the influence of the inductive line impedance in this range has been compensated by the virtual resistors. As observed in Fig. 8(b.1)–(b.3), the quadrature current sharing among the parallel inverters can be adjusted by regulating the q -axis virtual resistance ratio.

By contrast, the relationships of variables R_{vird} , I_{od} , and ω with different line impedances are derived by assigning R_{virq} and I_{oq} to certain values. The relationships of R_{vird} , I_{od} , and ω with zero, resistive–inductive, and purely inductive line impedance are shown in Fig. 9(a.1)–(a.3), respectively. Additionally, Fig. 9(b.1)–(b.3) is obtained by assuming R_{vird} to different values based on the relationships of R_{vird} , I_{od} , and ω under different line impedance conditions.

As observed from Fig. 9(b.1)–(b.3), the influence of direct output current on angular frequency changes by an exponential dependence when it gets closer to the resonance frequency of PR controller, which means that the impact of R_{vird} and I_{od} on ω can be neglected.

B. I_{od} Sharing

In order to share active loads, the parallel inverters will have different output voltage amplitude deviations from the voltage

amplitude reference $|V_{ref}|$, which depend on the output direct current and d -axis virtual resistance value of each inverter.

The voltage drop (ΔV) can be divided into two parts as follows:

$$\Delta V = I_{od}R_{vird} + |V_{ref}| [1 - |T_{plant}(j\omega'_0)|] \quad (12)$$

where the ω'_0 is the angular frequency of frequency-stable operation point.

The first part of (12) is the product of d -axis virtual resistance R_{vird} and direct current output I_{od} , which dominantly affects the output voltage amplitude drop. The second part of (12) is caused by the magnitude attenuation of closed-loop transfer function which results from the small but nonlinear frequency deviation due to the characteristic of PR controller. However, as discussed above, the system frequency will be stable and the deviations among the parallel inverters will be equal to each other, that is, the voltage deviations resulting from the second part of (12) are also the same among inverters. Therefore, the influence on the deviations can be neglected. Thus, the per-unit value of output voltage amplitude can be derived from (10) as follows:

$$\frac{|V_o|}{|V_{ref}|} = |T_{plant}(s)| = f(I_{od}, I_{oq}, R_{vird}, R_{virq}, \omega). \quad (13)$$

The parameters of R_{virq} and I_{oq} are fixed to analyze the relationship of R_{vird} , I_{od} , and V_o . The relationship of R_{vird} , I_{od} , and V_o with zero, resistive–inductive, and purely inductive line impedances are shown in Fig. 10. As it can be seen that the line impedances in the certain range barely have effect on the relationship of R_{vird} , I_{od} , and V_o . Fig. 10(b.1)–(b.3) shows the inherent $I_{od} - V_o$ droop mechanism of the proposed controller under different line impedance conditions. As observed, as the output direct current I_{od} increases, the voltage amplitude V_o decreases with different ratio corresponding to different R_{vird}

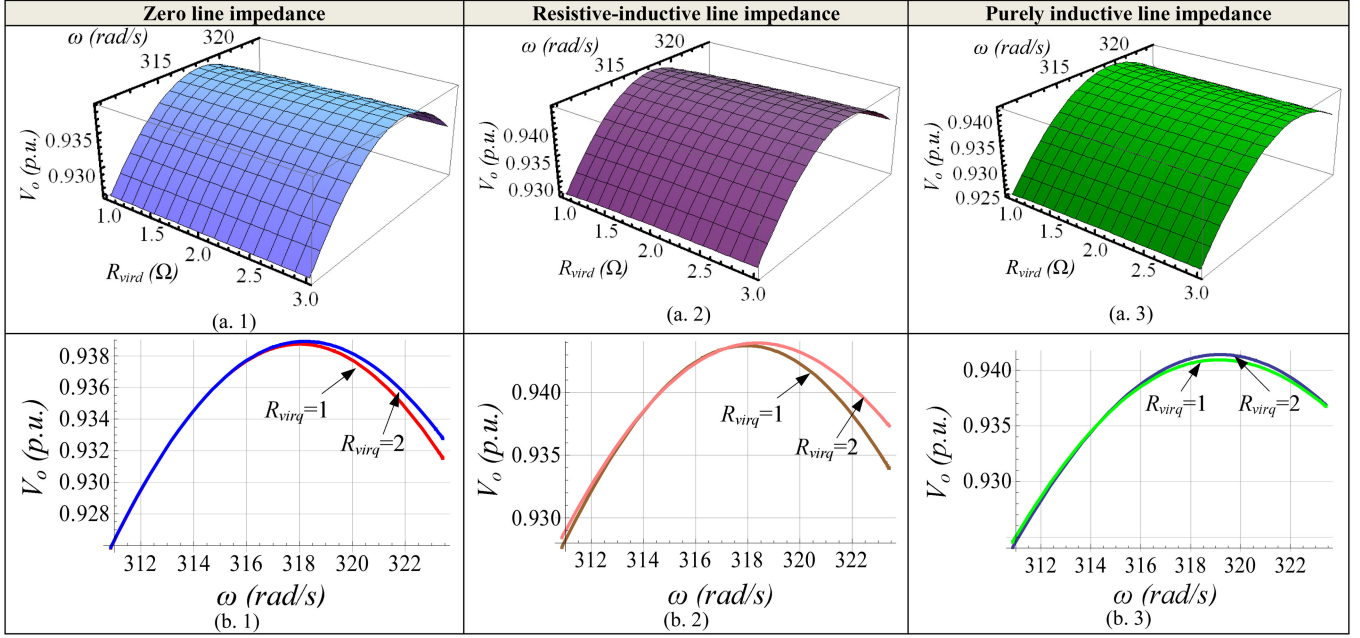


Fig. 11. Relationship of R_{virq} , ω , and V_o with different line impedances. (a) Relationship of R_{virq} , ω , and V_o with different line impedances. (b) Relationship of ω and V_o when $R_{virq} = 1\Omega/2\Omega$ with different line impedances, respectively.

values. Thus, the direct current sharing among the parallel inverters can be adjusted by regulating the d -axis virtual resistance ratio.

Similarly, R_{virq} , I_{od} are fixed to analyze the effect of frequency deviation on the voltage amplitude V_o with different line impedances. The relationships of R_{virq} , ω , and V_o with zero, resistive-inductive, and purely inductive line impedance are shown in Fig. 11(a.1)–(a.3), respectively. Fig. 11(b.1)–(b.3) indicates that the relationship $V_o - \omega$ almost immune to both R_{virq} and different line impedances. The effects of R_{virq} and ω on V_o are nonlinear but quite small in comparison with the voltage drop caused by adjusting R_{virq} and I_{od} . Considering that the voltage drop caused by $\Delta\omega$ is approximately the same in each inverter, it can be neglected.

Consequently, it can be observed a very well decoupling characteristic between I_{od} and I_{oq} for a large set of X/R ratios (from purely X to purely R).

C. Virtual Impedance Design

The virtual impedances in the proposed control loop are used to generate the direct and quadrature voltage deviations by multiplying the direct or quadrature currents separately. The direct and quadrature voltage deviations are used to automatically adjust the amplitude and phase angular of inverter output voltage. Given that virtual impedances induce output voltage and frequency deviation, they should be chosen to ensure that the voltage and frequency deviations are in the permissible range. For example, the maximum voltage deviation (ΔV_{max}) is 10%, while the maximum frequency deviation (Δf_{max}) is 0.5 Hz in a low-voltage network.

The relationship between the maximum voltage magnitude deviation ΔV_{dmax} and I_{od} can be derived as follows:

$$\Delta V_{dmax} = R_{virq} \cdot I_{od}. \quad (14)$$

In an extreme case, the inverter is assumed to supply only active current. (1) can be presented as follows:

$$\Delta V_{max} = R_{virq_max} \cdot I_{od_max} \quad (15)$$

where I_{od_max} is the maximum d -axis current of the inverter.

Thus, the upper limitation of the d -axis virtual resistor can be described as follows:

$$R_{virq_max} = \Delta V_{max} / I_{od_rate}. \quad (16)$$

Similarly, in an extreme case, the inverter is assumed to supply only reactive current. The relationship between the maximum angular frequency ω_{max} , quadrature output current I_{oq} , and R_{virq} can be derived from (11) as

$$R_{virq_max} = \frac{\text{num}}{\text{den}} \quad (17)$$

being

$$\begin{aligned} \text{num} &= V_{ref} \omega_{max} (\omega_{max}^2 - \omega_o^2) [K_{iv} (1 + C_f L_f \omega_{max}^2) \\ &+ C_f K_{pv} (K_{pi} K_{PWM} + r) (\omega_{max}^2 - \omega_o^2)] \\ \text{den} &= I_{oq_max} K_{pi} K_{PWM} [\omega_{max}^2 (K_{iv}^2 + K_{pv}^2 \omega_{max}^2) \\ &+ K_{pv}^2 \omega_o^2 (\omega_o^2 - 2\omega_{max}^2)] \end{aligned}$$

where V_{ref} is the voltage reference magnitude, ω_o is the fundamental frequency, K_{PWM} is the gain of three-phase inverter, and I_{oq_max} is the maximum q -axis current output of the inverter.

This relationship is more complex than the relationship of ΔV_{dmax} , I_{od_max} , and R_{virq_max} because the frequency of the proposed system is affected not only by the virtual resistance and quadrature current but also by the PR voltage control loop. Based on (17), the maximum q -axis virtual resistance can be calculated.

On the other hand, another functionality of the virtual resistance is to compensate the effects of line inductance. Thus, the

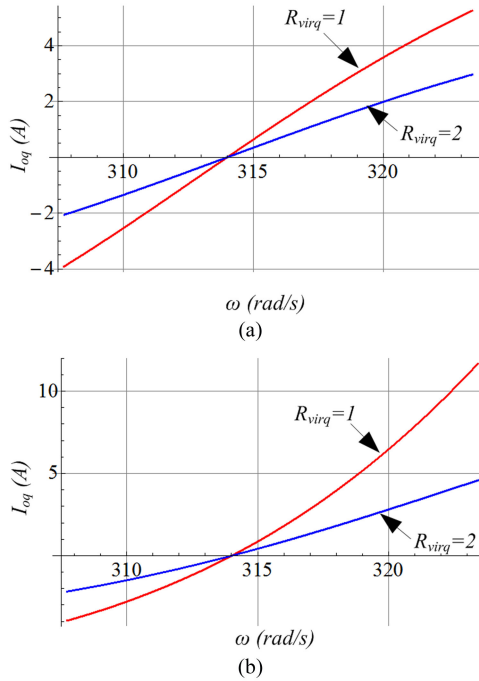


Fig. 12. Relationship of I_{oq} and ω when the line impedances are equal to the maximum values. (a) L_{line} is equal to 6 mH. (b) R_{line} is equal to 15 Ω .

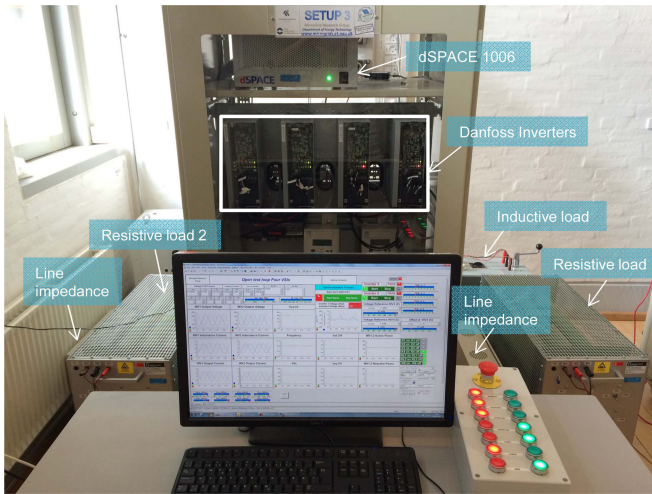


Fig. 13. Experimental setup.

virtual resistor should not be too small to predominate over the output impedance of the converter.

D. limitations of the Line Impedance

The limitations of the line impedance depend on the control loop parameters, the virtual impedance, and electrical parameters. In this case, if the $R_{vir d}$ and $R_{vir q}$ are both equal to 2 Ω , the maximum inductive line impedance and the maximum resistive line impedance that are able to maintain the steady-state operation of the proposed parallel-inverter-based system can be calculated by (11). The maximum inductive line impedance and the maximum resistive line impedance are approximately 6 mH and 15 Ω , respectively. The proposed $I_{od} - V_o$ and $I_{oq} - \omega$ droop

TABLE I
POWER STAGE AND CONTROL SYSTEM PARAMETERS

Parameters	Description	Value	
DG Inverter and output filter	V_{dc}	DC voltage	650 V
	V_{MG}	MG voltage	311 V
	f	MG frequency	50 Hz
	f_s	Switching frequency	10 kHz
	L_f	Filter inductance	1.8 mH
	C_f	Filter capacitance	25 μ F
	L_{line1}	Resistive-inductive line	1 Ω + 1.7 mH
	L_{line2}	Inductive line	1.8 mH
Loads (see Figs. 16 and 17)	Z_{load1}	Local load 1	57 + j2.83 Ω
	Z_{load2}	Local load 2	57 Ω
Inner Loop	k_{pi}	Current proportional term	0.07
	K_{ii}	Current integral term	0
	K_{pv}	Voltage proportional term	0.04
	K_{iv}	Voltage integral term	94
Droop Control	k_{pP}	Active power droop proportional coefficient	5e-7
	k_{iP}	Active power droop integral coefficient	6e-6
	k_{pQ}	Reactive power droop proportional coefficient	1e-5
	k_{iQ}	Reactive power droop integral coefficient	0
	R_v	Virtual resistance	2 Ω
	L_v	Virtual inductance	8 mH
Proposed Control	K_{p_PLL}	PLL proportional term	1.4
	K_{i_PLL}	PLL integral coefficient	1000
	$R_{vir d1}$	d-axis virtual resistance (inverter 1)	2 Ω
	$R_{vir q1}$	q-axis virtual resistance (inverter 1)	2 Ω
	$R_{vir d2}$	d-axis virtual resistance (inverter 2)	2 Ω
	$R_{vir q2}$	q-axis virtual resistance (inverter 2)	2 Ω
Loads (see Figs. 14 and 15)	Z_{load}	Local load 1	230 + j2.83 Ω
	Z_{test}	Step-up load	460 Ω

characteristics will present nonlinear when the line impedance over the limitations, as illustrated in Fig. 12.

In general, the proposed control strategy can provide good control performance over a wide range of line impedance which is hard to achieve by previously developed control strategies.

VI. EXPERIMENTAL RESULTS

An islanded experimental MG setup, which consists of three Danfoss 2.2-kW inverters, a real-time dSPACE1006 platform, LC filters, line impedance, resistive load, and resistance-inductance load has been built according to Fig. 1, as shown in Fig. 13. The switching frequency is set to 10 kHz. The electrical setup and control system parameters are listed in Table I. Different scenarios have been considered to test the performances of the proposed controller. In addition, a two parallel-inverters system has been used to compare and evaluate the performance of the proposed control approach with the conventional droop control. In this comparison, the parameters of electrical and inner voltage and current loops are all the same for both control methods.

A. Comparison Experiment With Inductive Line Impedance

Fig. 14 shows the experimental results to compare the control performance of the conventional droop control and the

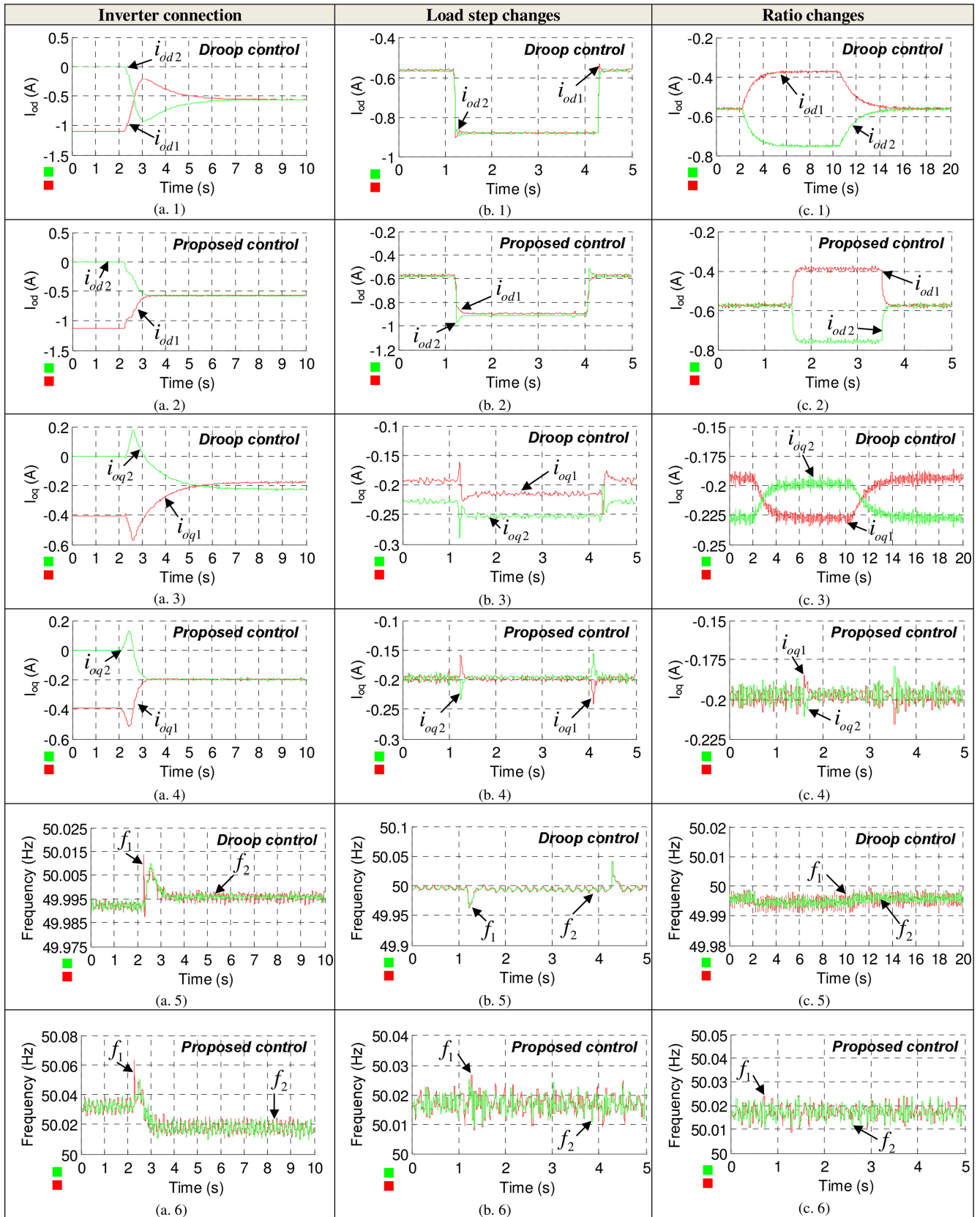


Fig. 14. Comparison experimental results with purely inductive line impedance in different scenarios.

proposed control with purely inductive line impedance which is equal to 1.8 mH in three different scenarios. Fig. 14(a.1)–(a.6) shows the transient response when VCI #2 is connected to VCI #1 with the conventional droop controller and the proposed controller separately. As seen in Fig. 14(a.1)–(a.4), VCI #1 is connected to a resistive–inductive load feeding around $(1.16+j0.4)$ A, while VCI #2 is disconnected. At 2.3 s, VCI #2 is connected to VCI #1, operating in parallel supplying a common load. The direct and quadrature currents output of VCI #2 are increased by 0.58 and 0.2 A, respectively, whereas the output direct and quadrature currents of the VCI #1 are decreased also by 0.58 and 0.2 A, respectively. The settling time is approximately 5.2 s with the conventional droop control, whereas the settling time is approximately 1 s with the proposed control strategy. Note that a small overshoot occurs due to small voltage error between inverters at the moment of connection, as shown in Fig. 14(a.3). An offset approximately 0.03 A of reactive current when using the droop control can be found in Fig. 14(a.3) due to the unbalance between line impedances, which is well suppressed when using the proposed controller as shown in Fig. 14(a.4). Fig. 14(a.5) shows that after 1.2 s, the system frequency at 49.992 Hz was restored closely to 49.996 Hz because of the decrease of the output currents with conventional droop control. As can be observed in Fig. 14(a.6), the system frequency at 50.035 Hz was restored to 50.018 Hz. All these deviations in both cases are maintained within the acceptable range, e.g., ± 0.5 Hz.

Fig. 14(b.1)–(b.6) shows the transient response during load step changes in the ac common bus. At the beginning, the parallel VCIs operate with same power rates. At 1.3 s, an extra 460- Ω resistive load is connected to the common bus. The direct currents output of VCI #1 and VCI #2 both increase by 0.31 A immediately to supply the needed current with the conventional droop control and the proposed controller as shown in Fig. 14(b.1) and (b.2). The quadrature currents output of VCI #1 and VCI #2 with the conventional droop control deviate by approximately 0.03 A because of the coupling between direct and quadrature currents as shown in Fig. 14(b.3). However, by using the proposed method, the quadrature currents output of VCI #1 and VCI #2 can maintain their original values, being barely affected by the direct output current disturbances as shown in Fig. 14(b.4). The frequency response to load disturbances for both VCI units is depicted in Fig. 14(b.5) and (b.6).

The transient response for sudden direct currents sharing ratio changes between the parallel VCIs is illustrated in Fig. 14(c.1)–(c.6). At the beginning, the VCI units parallel operate with a common RL load. Both the VCI #1 and VCI #2 feeds are approximately 0.58 A of direct current and 0.2 A of quadrature current. At 2.3 s, the direct current sharing ratio between the parallel VCIs with the conventional droop control has been suddenly changed from 1:1 to 1:2, and, then, changed back to 1:1 at 10.6 s. As it can be seen in Fig. 14(c.1), after about maximum 6 s, the output currents of the parallel VCIs are changed according to the new sharing ratio. Meanwhile, the quadrature current sharing has been affected by the changes on direct current sharing ratio as shown in Fig. 14(c.3). By contrast, the direct current sharing ratio between the parallel VCIs with the proposed con-

rol approach has also been suddenly changed from 1:1 to 1:2 at 1.6 s, and, then, changed back to 1:1 at 3.5 s. Fig. 14(c.2) shows that the direct current outputs of VCIs increase immediately according to the sharing ratio changes, and the transient response only lasts 0.2 s. Meanwhile, the quadrature current sharing ratio is kept constant via the decoupling control of the proposed controller.

B. Comparison Experiment With Resistive–Inductive Line Impedance

Fig. 15 shows the experimental results in order to compare the conventional droop control and the proposed control, with resistive–inductive line impedance which is equal to 1Ω plus 1.7 mH in three different scenarios. Similarly, Fig. 15(a.1)–(a.6) shows the transient response of direct currents, quadrature currents, and frequency when the VCI #2 is connected to VCI #1 with the conventional droop controller and the proposed controller separately. Fig. 15(b.1)–(b.6) illustrates the transient response for load step-up changes on ac common bus. Fig. 15(c.1)–(c.6) presents the transient response during sudden direct currents sharing ratio changes between the parallel VCIs. Both the conventional droop control and the proposed controller can achieve stable operation. By contrast, the proposed approach can endow the system with faster response speed, smaller overshoot, and decoupling control. Oscillation appears in the output current and system frequency with the conventional droop control due to the resistive–inductive line impedance and the coupling between I_{od} and I_{oq} .

When having almost zero line impedance, or highly resistive line impedance, the parallel VCIs cannot operate by using the conventional droop control. In contrast, an excellent performance can be obtained by using the proposed control as shown below.

For the rest of the tests, three-parallel inverters have been considered to test the performances of the proposed controller with zero line impedance in the following scenarios.

C. Hot-Swap Operation (Zero Line Impedance)

A three-parallel VCIs system sharing a linear load ($R_{load1} = 57 + j2.83 \Omega$) tests have been done to test individually the effects of DG units connecting and disconnecting. The transient response of the instantaneous currents, direct and quadrature output currents, and frequency with the proposed control are illustrated in Fig. 16(a), (b), and (c), respectively. As it can be observed, at the beginning, the three VCI units are on parallel operation with same power rates. At t_2 and t_3 , VCI #2 and VCI #3 are disconnected from VCI #1 separately, whereas VCI #1 is responsible for supplying the total current. Fig. 16 indicates that the output currents of VCI #2 and VCI #3 decrease to zero; meanwhile, the output currents of VCI #1 is increased to 7.5 A immediately. After the synchronization process, VCI #2 and VCI #3 are reconnected to VCI #1 at t_4 and t_5 , respectively. The transient performance is smooth and fast that the slowest settling time is about 0.8 s. Furthermore, the current oscillations are well damped.

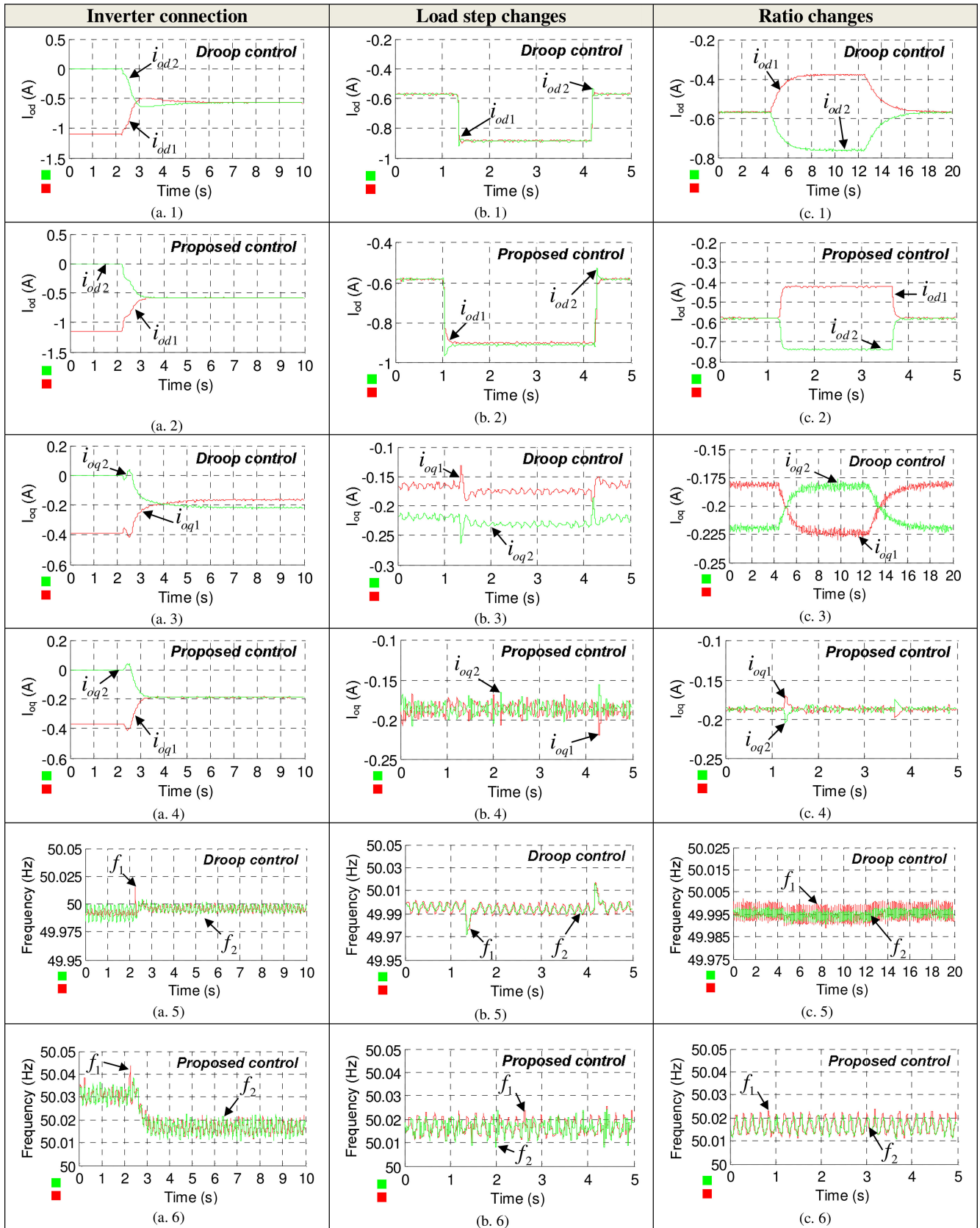


Fig. 15. Comparison experimental results with resistive-inductive line impedance in different scenarios.

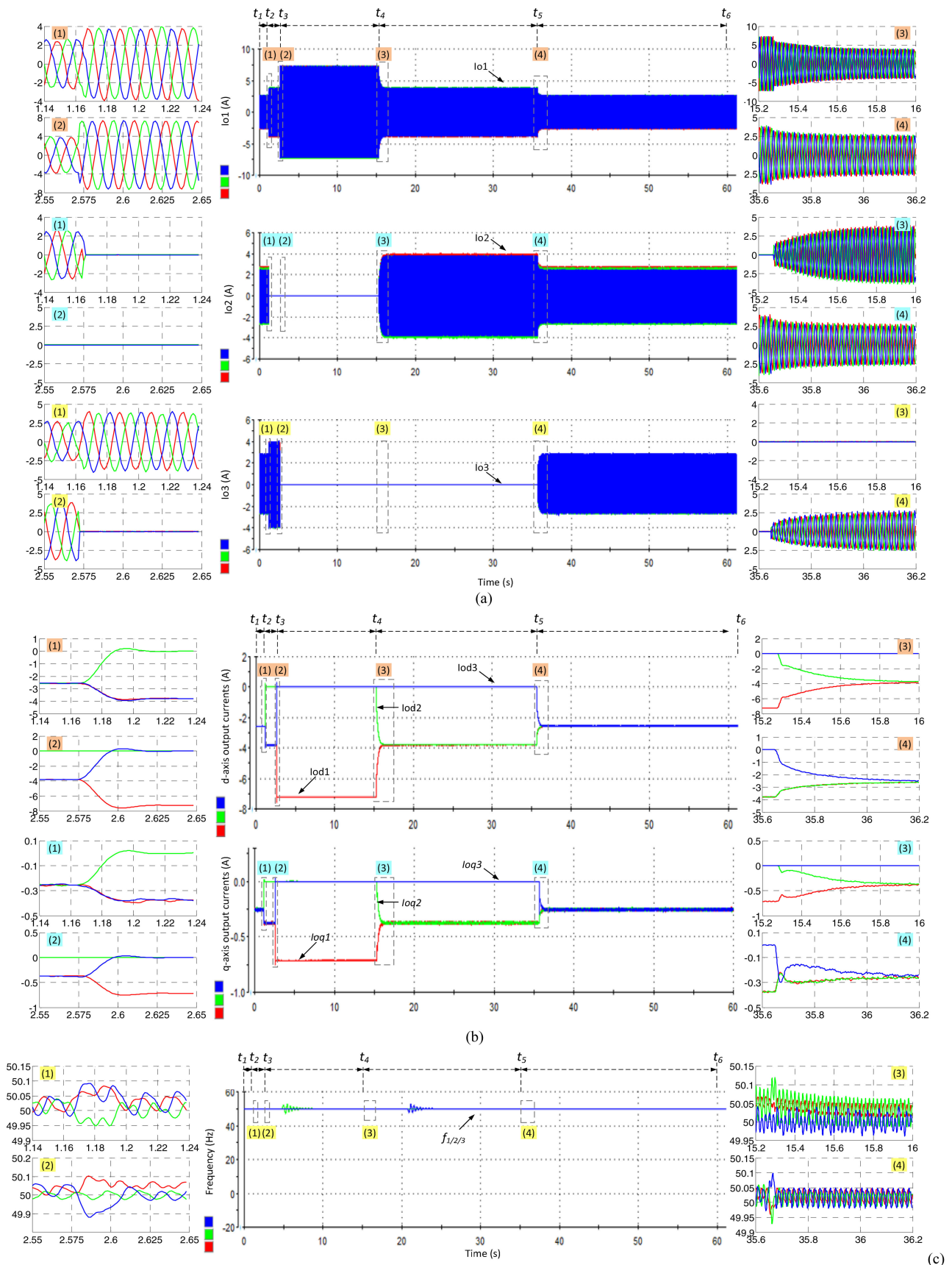


Fig. 16. Transient responses of VCI #1, VCI #2, and VCI #3 in connection and disconnection scenarios with the proposed controller. (a) Instantaneous output currents of VCI #1-#3. (b) Direct and quadrature output currents of VCI #1-#3. (c) Frequency of VCI #1-#3.

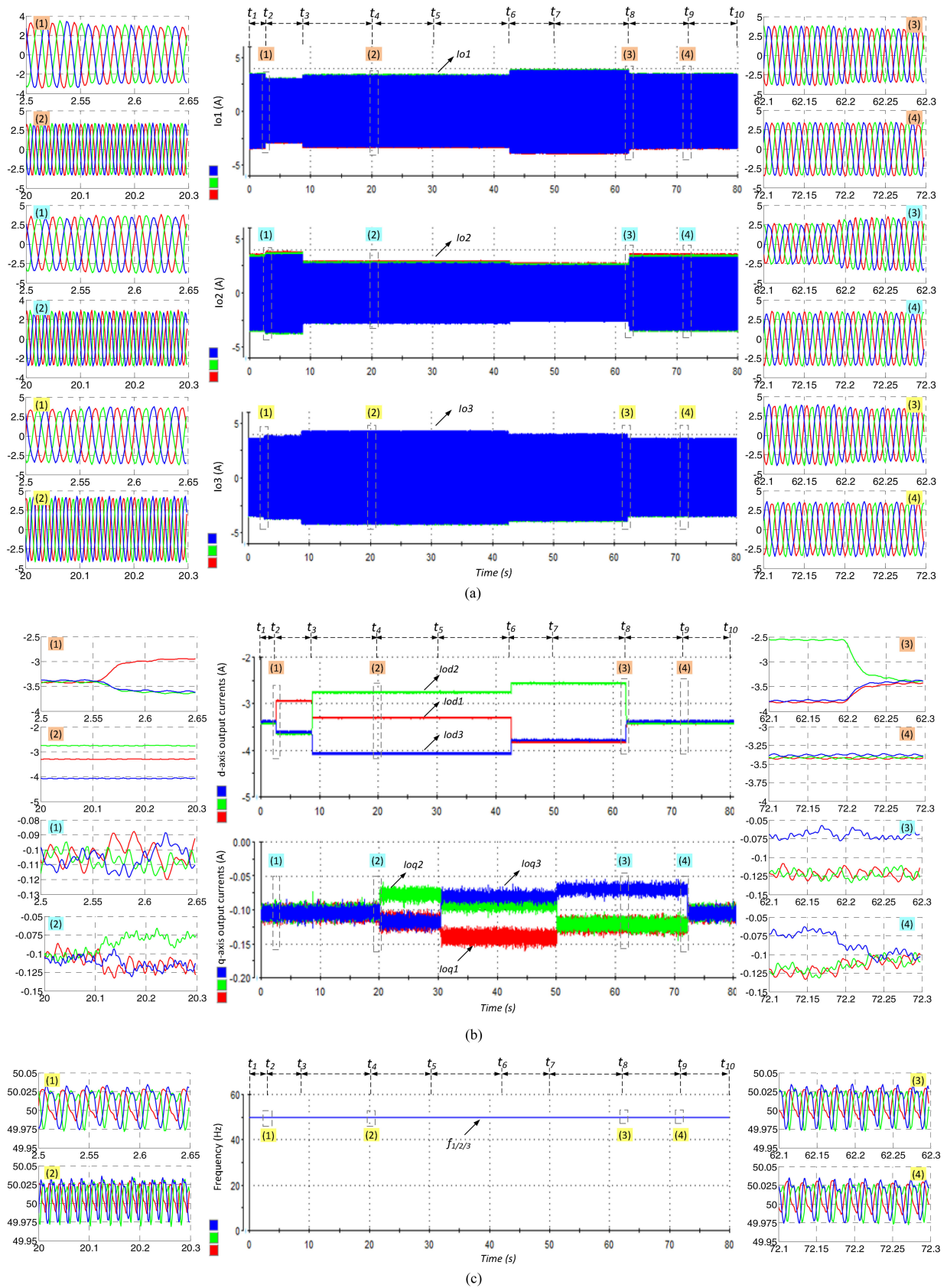


Fig. 17. Transient responses of VCI #1, VCI #2, and VCI #3 with different sharing ratios. (a) Instantaneous output currents of VCI #1-3. (b) Direct and quadrature output currents of VCI #1-3. (c) Frequency of VCI #1-3.

TABLE II
PERFORMANCE COMPARISON

	Purely inductive line impedance		Resistive–inductive line impedance		Zero or resistive line impedance	
	P - f/Q - V droop	Proposed control	P - f/Q - V droop	Proposed control	P - f/Q - V droop	Proposed control
Control capability	Yes	Yes, but cannot work with large inductive line impedance	Yes	Yes	No, need change to P - V/Q - f droop	Yes
Transient response	Slow	fast	Slow	fast	Slow	fast
Control performance	Good	Good, but cannot work with large inductive line impedance	Oscillations	Good	Good (if with P - V/Q - f droop)	Very well
Robustness	Poor	Good	Poor	Good	Poor	Good
Control parameters	m, n, Z_{vir}	$R_{vir d}, R_{vir q}$	m, n, Z_{vir}	$R_{vir d}, R_{vir q}$	m, n, Z_{vir}	$R_{vir d}, R_{vir q}$

D. Direct and Quadrature Currents Decoupling Sharing With Different Sharing Ratio (Zero Line Impedance)

In some cases, the parallel-connected VCIs need to supply active and reactive currents with different rates based on different power rates, requirements from EMS, or other superior control loops. A three-parallel VCIs setup sharing a common distributed linear load ($R_{load1} = 57 + j2.83 \Omega$) has been built to test the decoupling sharing performance of direct and quadrature currents with different sharing ratios. As shown in Fig. 17, the experiment can be divided into nine stages. The different stages (S1 to S9) are described as follows:

- 1) $S1 (t_1-t_2)$: The three VCIs are on parallel operation to share the common load equally due to the same virtual resistances.
- 2) $S2 (t_2-t_3)$: The d -axis virtual resistance ($R_{vir d}$) ratio of these three-paralleled VCIs is suddenly changed from 1:1:1 to 1.25:1:1 at t_2 . Thus, the direct current output of VCI #1 is decreased immediately, whereas the direct currents output of VCI #2 and VCI #3 are all increased by the same value within 0.1 s. The change on active current does not influence on the quadrature currents of these three VCIs as the theoretical analysis.
- 3) $S3 (t_3-t_4)$: The $R_{vir d}$ ratio is suddenly changed from 1.25:1:1 to 1.25:1.5:1 at t_3 . As observed, the output direct current of VCI #2 is decreased to the desired value.
- 4) $S4 (t_4-t_5)$: At t_4 , the paralleled system is subjected to a 50% step up in the q -axis virtual resistance ($R_{vir q}$) of VCI #2. Thus, the $R_{vir q}$ ratio of these three VCIs is suddenly changed from 1:1:1 to 1:1.5:1. As observed, the output quadrature current ratio becomes 1.5:1:1.5 which is the inverse proportion of the virtual resistance ratio as the theoretical analysis. In addition, the change on reactive current also does not affect the direct currents.
- 5) $S5 (t_5-t_6)$: The $R_{vir q}$ ratio suddenly changes from 1:1.5:1 to 1:1.5:1.75 at t_5 .
- 6) $S6 (t_6-t_7)$: At t_6 , the $R_{vir d}$ of VCI #1 reduces back to 2 Ω . Thus, the output direct current sharing ratio becomes 1.5:1:1.5.
- 7) $S7 (t_7-t_8)$: At t_7 , the $R_{vir q}$ of VCI #2 reduces back to 2 Ω . Hence, the direct current sharing ratio becomes 1.75:1.75:1.
- 8) $S8 (t_8-t_9)$: The $R_{vir d}$ ratio changes from 1:1.5:1 to 1:1:1 at t_8 .

- 9) $S9 (t_9-t_{10})$: The $R_{vir q}$ ratio changes from 1:1:1.75 to 1:1:1 at t_9 . Therefore, the output direct and quadrature currents of three VCIs are equal again.

The proposed controller successfully regulates the output currents of paralleled VCIs to the desired value. As can be observed, even with different power rates, the VCI units with the proposed control strategy will still maintain stable operation and achieve the online sharing ratio change. The proposed controller presents large stability margin to the control variables $R_{vir d}$ and $R_{vir q}$.

In summary, the experimental results reveal that the proposed control strategy does apply to low-voltage parallel-VCI-based system where the line impedance usually presents high ratio of R/X and short length because of its faster response speed, online sharing ratio change function, larger stability margin, smaller overshoot, plug “n” play operation, and decoupling control. In addition, the proposed control strategy also works well with inductive–resistive line impedance and small purely inductive line impedance by means of virtual resistor. The proposed $I_{od} - V_o$ and $I_{oq} - \omega$ droop characteristics will present non-linear when the line impedance over the limitations. Thus, the droop control strategy should be applied to the high-inductive system. In other cases, the proposed control strategy can provide superior performances. The prominent features of the proposed strategy compared with the conventional droop control are summarized in Table II.

VII. CONCLUSION AND FUTURE WORK

A simpler and faster controller that comprises a PLL, a virtual resistance loop, and a PR controller in inner voltage loop for controlling direct and quadrature load currents separately among parallel-three-phase inverters is developed. Based on the steady-state characteristic analysis, by adjusting the d -axis virtual resistance ratio between the parallel inverters, the direct load current sharing can be achieved, whereas by modifying the q -axis virtual resistance ratio between parallel inverters, the quadrature load current provided will be changed proportionally. The proposed control strategy does apply to low-voltage MGs and islanded minigrids. In addition, it can also works well with inductive–resistive line impedance and even small purely inductive line impedance thanks to the use of virtual resistance. Compared with conventional droop control, the described method does not need to calculate active and reactive powers. Thus, the method exhibits faster transient response and better precision.

$$G(s) = \frac{G_v(s)G_i(s)K_{P\text{PWM}}}{L_f C_f s^2 + (rC_f + G_i(s)K_{P\text{PWM}}C_f)s + 1 + G_v(s)G_i(s)K_{P\text{PWM}}} \quad (\text{A.2})$$

$$Z_o(s) = \frac{sL_f + r}{L_f C_f s^2 + (rC_f + G_i(s)K_{P\text{PWM}}C_f)s + 1 + G_v(s)G_i(s)K_{P\text{PWM}}} \quad (\text{A.3})$$

$$G_v(s) = K_{pv} + \frac{K_{iv}s}{s^2 + \omega_c^2} \quad (\text{A.4})$$

$$G_i(s) = K_{pi} \quad (\text{A.5})$$

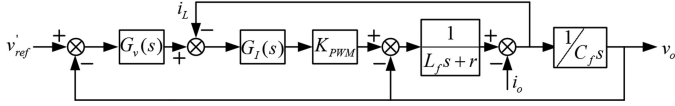


Fig. A.1. Block diagram of the dual-loop control.

Experimental results are included to show the excellent behavior of the proposed controller. The small-signal model and stability analysis will be presented in Part II of this paper.

APPENDIX

The detailed derivative process of (10) in Section IV is shown as follows.

As indicated in Fig. 5, the closed loop includes three-leg three-phase inverter, $L_f - C_f$ filter, line impedance, inner voltage and current control, and virtual resistance loop.

The block diagram of the inner current and voltage loops as well as the LC filter is shown in Fig. A.1.

Based on the diagram, the closed-loop transfer function can be written as follows:

$$v_o(s) = G(s)v_{\text{ref}}'(s) - Z_o(s)i_o(s) \quad (\text{A.1})$$

being (A.2–A.5) shown at the top of the page.

where $G(s)$ presents the tracking performance of the output voltage following the voltage reference, $Z_o(s)$ is the equivalent output impedance of the inverter, $v_o(s)$ is the output voltage, $v_{\text{ref}}'(s)$ is the reference voltage of inner voltage loop, $i_o(s)$ is the output current, $G_v(s)$ is the PR voltage control loop, $G_i(s)$ is the proportional current control loop, $K_{P\text{PWM}}$ is the gain of three phase inverter, L_f , C_f , and r are the inductor, capacitor, and inductor ESR of the LC filter, respectively, K_{pv} and K_{iv} are the proportional and integral coefficients of voltage control loop, ω_c is the resonant frequency of the PR regulator in voltage control loop, and K_{pi} is the proportional coefficients of current control loop.

To obtain the direct and quadrature load currents, the equivalent parallel connected resistive–inductive load can be represented as follows:

$$G_{L\text{equ}}(s) = \frac{1}{R_{L\text{equ}}} + \frac{1}{sL_{L\text{equ}}} \quad (\text{A.6})$$

where $G_{L\text{equ}}(s)$ is the equivalent load admittance, $R_{L\text{equ}}$ is the equivalent resistor, and $L_{L\text{equ}}$ is the equivalent inductance.

The line impedance can be expressed as follows:

$$Z_{\text{line}}(s) = R_{\text{line}} + sL_{\text{line}} \quad (\text{A.7})$$

where $Z_{\text{line}}(s)$ is the line impedance, R_{line} is the line resistor, and L_{line} is the line inductance.

Hence, the closed-loop transfer function $T_{\text{plant}}(s)$ can be derived based on Fig. 5

$$T_{\text{plant}}(s) = \frac{v_o(s)}{v_{\text{ref}}(s)} = \frac{G(s) [1 + G_{L\text{equ}}(s)Z_{\text{line}}(s)]}{1 + G_{L\text{equ}}(s)Z_{\text{line}}(s) + G_{\text{vir}}(s)G(s) + G_{L\text{equ}}(s)Z_o(s)} \quad (\text{A.8})$$

being

$$G_{\text{vir}}(s) = \frac{R_{\text{vir}d}}{R_{L\text{equ}}} + \frac{R_{\text{vir}q}}{sL_{L\text{equ}}}. \quad (\text{A.9})$$

REFERENCES

- [1] R. H. Lasseter, "MicroGrids," in *Proc. IEEE Power Eng. Soc. Winter Meet.*, 2002, vol. 1, pp. 305–308.
- [2] J. M. Guerrero, M. Chandorkar, T. Lee, and P. C. Loh, "Advanced control architectures for intelligent microgrids—Part I: Decentralized and hierarchical control," *IEEE Trans. Ind. Electron.*, vol. 60, no. 4, pp. 1254–1262, Apr. 2013.
- [3] P. Piagi and R. H. Lasseter, "Autonomous control of microgrids," presented at the *IEEE Power Engineering Society General Meet.*, Montreal, Canada, 2006.
- [4] Y. Li, D. M. Vilathgamuwa, and P. C. Loh, "Design, analysis, and real-time testing of a controller for multibus microgrid system," *IEEE Trans. Power Electron.*, vol. 19, no. 5, pp. 1195–1204, Sep. 2004.
- [5] J. M. Guerrero, L. Garcia De Vicuna, J. Matas, M. Castilla, and J. Miret, "Output impedance design of parallel-connected ups inverters with wireless load-sharing control," *IEEE Trans. Ind. Electron.*, vol. 52, no. 4, pp. 1126–1135, Aug. 2005.
- [6] J. C. Vasquez, J. M. Guerrero, A. Luna, and P. Rodriguez, "Adaptive droop control applied to voltage-source inverters operating in grid-connected and islanded modes," *IEEE Trans. Ind. Electron.*, vol. 56, no. 10, pp. 4088–4096, Oct. 2009.
- [7] J. Kim, J. M. Guerrero, P. Rodriguez, R. Teodorescu, and K. Nam, "Mode adaptive droop control with virtual output impedances for an inverter-based flexible AC microgrid," *IEEE Trans. Power Electron.*, vol. 26, no. 3, pp. 689–701, Mar. 2011.
- [8] R. H. Lasseter and P. Piagi, "Microgrid: A conceptual solution," in *Proc. IEEE Power Electron. Spec. Conf.*, Aachen, Germany, 2004, pp. 4285–4290.
- [9] M. Marwali, J.-W. Jung, and A. Keyhani, "Control of distributed generation systems—Part II: Load sharing control," *IEEE Trans. Power Electron.*, vol. 19, no. 6, pp. 1551–1561, Nov. 2004.
- [10] F. Katiraei and M. R. Irvani, "Power management strategies for a microgrid with multiple distributed generation units," *IEEE Trans. Power Syst.*, vol. 21, no. 4, pp. 1821–1831, Nov. 2006.
- [11] M. C. Chandorkar, D. M. Divan, and R. Adapa, "Control of parallel connected inverters in standalone AC supply systems," *IEEE Trans. Ind. Appl.*, vol. 29, no. 1, pp. 136–143, Jan./Feb. 1993.

- [12] J. Guerrero, L. D. Vicuna, J. Matas, M. Castilla, and J. Miret, "A wireless controller to enhance dynamic performance of parallel inverters in distributed generation system," *IEEE Trans. Power Electron.*, vol. 19, no. 5, pp. 1205–1213, Sep. 2004.
- [13] S. M. Ashabani and Y. A.-R. I. Mohamed, "New family of microgrid control and management strategies in smart distribution grids—Analysis, comparison and testing," *IEEE Trans. Power Syst.*, vol. 29, no. 5, pp. 2257–2269, Sep. 2014.
- [14] C. Sao and P. Lehn, "Autonomous load sharing of voltage source converters," *IEEE Trans. Power Del.*, vol. 20, no. 2, pp. 1009–1016, Apr. 2005.
- [15] Y. A.-R. I. Mohamed and E. F. El-Saadany, "Adaptive decentralized droop controller to preserve power sharing stability of paralleled inverters in distributed generation microgrids," *IEEE Trans. Power Electron.*, vol. 23, no. 6, pp. 2806–2816, Nov. 2008.
- [16] Y. Guan, W. Wu, X. Guo, and H. Gu, "An improved droop controller for grid-connected voltage source inverter in microgrid," in *Proc. 2nd Int. Symp. Power Electron. Distrib. Gener. Syst.*, 2010, pp. 823–828.
- [17] S. J. Chiang, C. Y. Yen, and K. T. Chang, "A multimodule parallelable series-connected PWM voltage regulator," *IEEE Trans. Ind. Electron.*, vol. 48, no. 3, pp. 506–516, Jun. 2001.
- [18] Y. W. Li and C. N. Kao, "An accurate power control strategy for powerelectronics- interfaced distributed generation units operating in a low voltage multibus microgrid," *IEEE Trans. Power Electron.*, vol. 24, no. 12, pp. 2977–2988, Dec. 2009.
- [19] A. Engler and N. Sultanis, "Droop control in LV-grids," presented at the Int. Conf. Future Power Systems, Amsterdam, The Netherlands, Nov. 2005.
- [20] J. M. Guerrero, J. Matas, L. G. de Vicuna, M. Castilla, and J. Miret, "Decentralized control for parallel operation of distributed generation inverters using resistive output impedance," *IEEE Trans. Ind. Electron.*, vol. 54, no. 2, pp. 994–1004, Apr. 2007.
- [21] H. Laaksonen, P. Saari, and R. Komulainen, "Voltage and frequency control of inverter based weak LV network microgrid," presented at the Int. Conf. Future Power Systems, Amsterdam, The Netherlands, Nov. 18, 2005.
- [22] K. D. Brabandere, B. Bolsens, J. V. Denkeybus, A. Woyte, J. Driesen, and R. Belmans, "A voltage and frequency droop control method for parallel inverters," *IEEE Trans. Power Electron.*, vol. 22, no. 4, pp. 1107–1115, Jul. 2007.
- [23] T. L. Vandoorn, B. Meersman, J. D. M. De Kooning, and L. Vandevelde, "Directly-coupled synchronous generators with converter behavior in islanded microgrids," *IEEE Trans. Power Syst.*, vol. 27, no. 3, pp. 1395–1406, Aug. 2012.
- [24] W. Yao, M. Chen, J. M. Guerrero, and Z.-M. Qian, "Design and analysis of the droop control method for parallel inverters considering the impact of the complex impedance on the power sharing," *IEEE Trans. Ind. Electron.*, vol. 58, no. 2, pp. 576–588, Feb. 2011.
- [25] T. L. Vandoorn, J. D. M. De Kooning, B. Meersman, J. M. Guerrero, and L. Vandevelde, "Voltage-Based control of a smart transformer in a microgrid," *IEEE Trans. Ind. Electron.*, vol. 60, no. 4, pp. 1291–1305, Apr. 2013.
- [26] E. Rokrok and M. E. H. Golshan, "Adaptive voltage droop method for voltage source converters in an islanded multibus microgrid," *IET Gener., Transmiss., Distrib.*, vol. 4, no. 5, pp. 562–578, 2010.
- [27] G. Diaz, C. Gonzalez-Moran, J. Gomez-Aleixandre, and A. Diez, "Scheduling of droop coefficients for frequency and voltage regulation in isolated microgrids," *IEEE Trans. Power Syst.*, vol. 25, no. 1, pp. 489–496, Feb. 2010.
- [28] R. Majumder, B. Chaudhuri, A. Ghosh, R. Majumder, G. Ledwich, and F. Zare, "Improvement of stability and load sharing in an autonomous microgrid using supplementary droop control loop," *IEEE Trans. Power Syst.*, vol. 25, no. 2, pp. 796–808, May 2010.
- [29] C.-T. Lee, C.-C. Chu, and P.-T. Cheng, "A new droop control method for the autonomous operation of distributed energy resource interface converters," *IEEE Trans. Power Electron.*, vol. 28, no. 4, pp. 1980–1993, Apr. 2013.
- [30] T. L. Vandoorn, B. Meersman, L. Degroote, B. Renders, and L. Vandevelde, "A control strategy for islanded microgrids with DC-Link voltage control," *IEEE Trans. Power Del.*, vol. 26, no. 2, pp. 703–713, Apr. 2011.
- [31] E. A. A. Coelho, P. C. Cortizo, and P. F. D. Garcia, "Small-signal stability for parallel-connected inverters in stand-alone AC supply systems," *IEEE Trans. Ind. Appl.*, vol. 38, no. 2, pp. 533–542, Mar./Apr. 2002.
- [32] J. C. Vasquez, J. M. Guerrero, M. Savaghebi, J. Eloy-Garcia, and R. Teodorescu, "Modeling, analysis, and design of stationary-reference frame droop-controlled parallel three-phase voltage source inverters," *IEEE Trans. Ind. Electron.*, vol. 60, no. 4, pp. 1271–1280, Apr. 2013.
- [33] C. Sao and P. Lehn, "Control and power management of converter fed microgrids," *IEEE Trans. Power Syst.*, vol. 23, no. 3, pp. 1088–1098, Aug. 2008.
- [34] C. Sao and P. W. Lehn, "Autonomous load sharing between converters and generators in microgrids," presented at the IEEE Power Energy Society General Meet., San Diego, CA, USA, Jul. 24–29, 2011.
- [35] E. K. Sato, A. Kawamura, and R. Fujii, "Theoretical and experimental verification of independent control for parallel-connected multi-UPS's," in *Proc. 25th Telecommun. Energy Conf.*, Yokohama, Japan, Oct. 2003, pp. 485–492.
- [36] E. K. Sato and A. Kawamura, "Decentralized control for redundant parallelism of uninterruptible power supplies with different ratings using only current sensors," in *Proc. IEEE 36th Power Electron. Spec. Conf.*, Recife, Brazil, Jun. 2005, pp. 2823–2829.
- [37] S. G. Mohammad and D. D. C. Lu, "A control method for inverter-based islanded microgrids based on v-i droop characteristics," *IEEE Trans. Power Del.*, vol. 30, no. 3, pp. 1196–1204, Jun. 2015.
- [38] K. De Brabandere, Voltage and frequency droop control in low voltage grids by distributed generators with inverter front-end, Ph.D. dissertation, Dept. Electr. Eng., Katholieke Univ. Leuven, Leuven, Belgium, Oct. 2006.
- [39] K. D. Wu, J. C. Wu, and H. L. Jou, "Simplified control method for parallel-connected DC/AC inverters," *IEE Proc. Electr. Power Appl.*, vol. 153, pp. 787–792, Dec. 4, 2006.
- [40] I. Batarseh, K. Siri, and H. Lee, "Investigation of the output droop characteristics of parallel-connected DC-DC converters," in *Proc. IEEE 25th Annu. Rec. Power Electron. Spec. Conf.*, Jun. 1994, vol. 2, pp. 1342–1351.
- [41] H. Kakigano, Y. Miura, T. Ise, and R. Uchida, "DC micro-grid for super high quality distribution—System configuration and control of distributed generations and energy storage devices," in *Proc. IEEE 37th Power Electron. Spec. Conf.*, Jun. 2006, pp. 1–7.
- [42] X. Lu, J. M. Guerrero, K. Sun, and J. C. Vasquez, "An improved droop control method for DC microgrids based on low bandwidth communication with DC bus voltage restoration and enhanced current sharing accuracy," *IEEE Trans. Power Electron.*, vol. 29, no. 4, pp. 1800–1812, Apr. 2014.
- [43] S. Golestan, M. Joorabian, H. Rastegar, A. Roshan, and J. M. Guerrero, "Droop based control of parallel-connected single-phase inverters in D-Q rotating frame," in *Proc. IEEE Int. Conf. Ind. Technol.*, Feb. 10–13, 2009, pp. 1–6.
- [44] P. Rodríguez, A. Luna, I. Candela, R. Mujal, R. Teodorescu, and F. Blaabjerg, "Multiresonant frequency-locked loop for grid synchronization of power converters under distorted grid conditions," *IEEE Trans. Ind. Electron.*, vol. 58, no. 1, pp. 127–138, Jan. 2011.
- [45] S.-K. Chung, "A phase tracking system for three phase utility interface inverters," *IEEE Trans. Power Electron.*, vol. 15, no. 3, pp. 431–438, May 2000.
- [46] X. Guo, W. Liu, X. Zhang, X. Sun, Z. Lu, and J. M. Guerrero, "Flexible control strategy for grid-connected inverter under unbalanced grid faults without PLL," *IEEE Trans. Power Electron.*, vol. 30, no. 4, pp. 1773–1778, Apr. 2015.
- [47] M. G. Josep, J. Matas, L. G. De Vicuña, M. Castilla, and J. Miret, "Wireless-control strategy for parallel operation of distributed-generation inverters," *IEEE Trans. Ind. Electron.*, vol. 53, no. 5, pp. 1461–1470, Oct. 2006.



Yajuan Guan (S'14) received the B.S. and M.S. degrees in electrical engineering from the Yanshan University, Qinhuangdao, Hebei, China, in 2007 and 2010, respectively. She is currently working toward the Ph.D. degree at the Department of Energy Technology, Aalborg University, Aalborg, Denmark, as part of the Denmark Microgrids Research Program.

From 2010 to 2012, she was an Assistant Professor with the Institute of Electrical Engineering, Chinese Academy of Sciences, Beijing, China, where since 2013, she has been a Lecturer. Her research interests

include microgrids, distributed generation systems, power converter for renewable energy generation systems, and ancillary services for microgrids.



Josep M. Guerrero (S'01–M'04–SM'08–F'15) received the B.S. degree in telecommunications engineering, the M.S. degree in electronics engineering, and the Ph.D. degree in power electronics from the Technical University of Catalonia, Barcelona, Spain, in 1997, 2000, and 2003, respectively.

Since 2011, he has been a Full Professor at the Department of Energy Technology, Aalborg University, Aalborg, Denmark, where he is responsible for the Microgrid Research Program; since 2012, he has been a Guest Professor at the Chinese Academy of

Science, Beijing, China, and the Nanjing University of Aeronautics and Astronautics, Nanjing, China; since 2014, he has been a Chair Professor at Shandong University, Jinan, China; and since 2015, he has been a Distinguished Guest Professor at Hunan University, Changsha, China. His research interests include different microgrid aspects, including power electronics, distributed energy-storage systems, hierarchical and cooperative control, energy management systems, and optimization of microgrids and islanded minigrids.

Prof. Guerrero is an Associate Editor of the *IEEE TRANSACTIONS ON POWER ELECTRONICS*, the *IEEE TRANSACTIONS ON INDUSTRIAL ELECTRONICS*, and the *IEEE INDUSTRIAL ELECTRONICS MAGAZINE*, and an Editor of the *IEEE TRANSACTIONS ON SMART GRID* and the *IEEE TRANSACTIONS ON ENERGY CONVERSION*. He has been a Guest Editor of the *IEEE TRANSACTIONS ON POWER ELECTRONICS* Special Issues: the Power Electronics for Wind Energy Conversion and the Power Electronics for Microgrids; the *IEEE TRANSACTIONS ON INDUSTRIAL ELECTRONICS* Special Sections: the Uninterruptible Power Supplies systems, the Renewable Energy Systems, the Distributed Generation and Microgrids, and the Industrial Applications and Implementation Issues of the Kalman Filter; and the *IEEE TRANSACTIONS ON SMART GRID* Special Issue on the Smart DC Distribution Systems. He was the Chair of the Renewable Energy Systems Technical Committee of the IEEE Industrial Electronics Society. In 2014, he received the award of Highly Cited Researcher by Thomson Reuters.



Xin Zhao received the B.S. and M.S. degrees in power electronics and electrical drives from Northwestern Polytechnical University, Xi'an, China, in 2010 and 2013, respectively. He is currently working toward the Ph.D. degree at the Department of Energy Technology, Aalborg University, Aalborg, Denmark.

His research interests include control of power converters, power quality, and microgrids.



Juan C. Vasquez (M'12–SM'14) received the B.S. degree in electronics engineering from the Autonomous University of Manizales, Manizales, Colombia, in 2004, and the Ph.D. degree in automatic control, robotics, and computer vision from the Technical University of Catalonia, Barcelona, Spain, in 2009.

He was with the Autonomous University of Manizales, where he taught courses on digital circuits, servo systems, and flexible manufacturing systems.

He was also with the Technical University of Catalonia, as a Postdoctoral Assistant, teaching courses based on renewable energy systems. From February 2015 to April 2015, he was a Visiting Scholar with the Center of Power Electronics Systems, Virginia Tech. In 2011, he was an Assistant Professor in microgrids, and he is currently an Associate Professor at the Department of Energy Technology, Aalborg University, Aalborg, Denmark. He is coresponsible of the Research Program in Microgrids. His current research interests include operation, power management, hierarchical control, and optimization and power quality applied to distributed generation and ac/dc microgrids.

Dr. Vasquez is currently a Member of the IEC System Evaluation Group SEG4 on LVDC Distribution and Safety for use in Developed and Developing Economies and the Renewable Energy Systems Technical Committee in the IEEE Industrial Electronics Society.



Xiaoqiang Guo (M'10–SM'14) received the B.S. and Ph.D. degrees in electrical engineering from Yanshan University, Qinhuangdao, China, in 2003 and 2009, respectively.

He has been a Postdoctoral Fellow with the Laboratory for Electrical Drive Applications and Research, Ryerson University, Toronto, ON, Canada. He is currently an Associate Professor at the Department of Electrical Engineering, Yanshan University. He has authored/coauthored more than 50 technical papers, in addition to nine patents. His current research inter-

ests include high-power converters and ac drives, electric vehicle charging station, and renewable energy power conversion systems.

Dr. Guo is a Senior Member of the IEEE Power Electronics Society and the IEEE Industrial Electronics Society. He is an active Referee for the *IEEE TRANSACTIONS ON SUSTAINABLE ENERGY*, the *IEEE TRANSACTIONS ON SMART GRID*, the *IEEE TRANSACTIONS ON INDUSTRIAL ELECTRONICS*, and the *IEEE TRANSACTIONS ON POWER ELECTRONICS*.